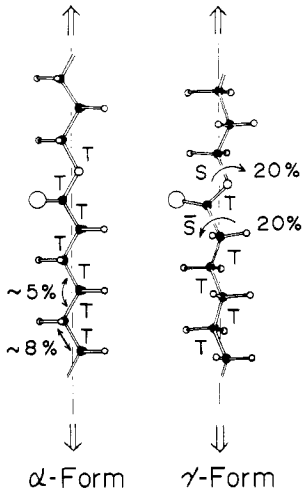

Figure 8. Calculated distribution of the strain energy when the nylon 6 chain is stretched along the chain axis.

lecular forces because the internal and external interactions do not strongly couple with one other. This is because the intermolecular interactions are almost restricted to the nonbonded methyl–methyl pairs and the skeletal chains are affected by the intermolecular interactions only through such side group interactions. In the case of the γ form nylon 6, the intermolecular forces influence directly the skeletal chains, different from the case of i-PP. A detailed discussion for i-PP will be reported soon.[15]

References and Notes

(1) Tashiro, K.; Kobayashi, M.; Tadokoro, H. *Macromolecules* **1978**, *11*, 908.
(2) Tashiro, K.; Kobayashi, M.; Tadokoro, H. *Macromolecules* **1978**, *11*, 914.
(3) Holmes, D. R.; Bunn, C. W.; Smith, D. J. *J. Polym. Sci.* **1955**, *17*, 159.
(4) Arimoto, H.; Ishibashi, M.; Hirai, M.; Chatani, Y. *J. Polym. Sci., Part A* **1965**, *3*, 317.
(5) Perker, J. P.; Lindenmeyer, P. H. *J. Appl. Polym. Sci.* **1977**, *21*, 821.
(6) Jakes, J.; Krimm, S. *Spectrochim. Acta, Part A* **1971**, *27a*, 19. Schachtschneider, J. H.; Snyder, R. G. *Spectrochim. Acta* **1963**, *19*, 117.
(7) Williams, D. E. *J. Chem. Phys.* **1967**, *47*, 4680. Kobayashi, M. *Ibid.* **1977**, *66*, 32.
(8) Itoh, K.; Shimanouchi, T. *J. Mol. Spectrosc.* **1972**, *42*, 86.
(9) Nye, J. F. "Physical Properties of Crystals"; Clarendon Press: London, 1957.
(10) Kaji, K. Doctoral Thesis, Kyoto University, 1970. *Sen'i To Kogyo* **1970**, *3*, 555.
(11) Ito, T.; Hirata, T.; Fujita, S. *J. Polym. Sci., Polym. Phys. Ed.* **1979**, *17*, 1237.
(12) Malta, V.; Cojazzi, G.; Fichera, A.; Ajó, D.; Zannetti, R. *Eur. Polym. J.* **1979**, *15*, 765.
(13) Natta, G.; Corradini, P. *Nuovo Cimento, Suppl.* **1960**, *15*, 33.
(14) Miyasaka, K.; Isomoto, T.; Koganeya, H.; Uehara, K.; Ishikawa, K. *J. Polym. Sci., Polym. Phys. Ed.* **1980**, *18*, 1047.
(15) Tashiro, K.; Kobayashi, M.; Tadokoro, H., submitted for publication.
(16) Schaufele, R. F.; Shimanouchi, T. *J. Chem. Phys.* **1967**, *47*, 3605.
(17) Strobl, G. R.; Eckel, R. *J. Polym. Sci., Polym. Phys. Ed.* **1976**, *14*, 913.
(18) Holliday, L.; White, J. W. *Pure Appl. Chem.* **1971**, *26*, 545.

Activation Energy Insensitivity to Barrier-Crossing Correlations in Long-Chain Molecules[1]

D. Perchak and J. H. Weiner*

Department of Physics and Division of Engineering, Brown University, Providence, Rhode Island 02912. *Received January 16, 1981*

ABSTRACT: Recent experiments by Morawetz et al. show that the activation energy for rotational barrier crossings in a long-chain molecule in solution is the same as for an analogue molecule with only a single rotational barrier. We present the results of computer simulation studies of this process which use the technique of Brownian dynamics applied to a model of a polymer chain regarded as a system of linked rigid bodies. The computer simulation results parallel qualitatively the experimental results of Morawetz et al. We consider also a model system with two degrees of freedom, each representing the motion of a dihedral angle, and a tensor viscosity which permits a controlled degree of correlation between the motion of these angles over rotational barriers. This model also exhibits insensitivity of the activation energy to the degree of correlation and an examination of its trajectories provides some insight into the process.

Introduction

A linear long-chain molecule in solution undergoes frequent conformational transitions by rotations about bonds of the backbone chain. These rotations are opposed by a rotational energy barrier (one associated with each bond) due to side-group interactions, and the overcoming of this barrier is a thermally activated process.

A question of long standing concerns the degree of correlation that exists among the times at which the various bonds along the chain undergo rotations over their respective barriers. That some correlation should exist is seen by considering the situation in which a rotation over the barrier takes place about a bond near the chain center while the dihedral angles describing the conformations of the remaining bonds remain unchanged. In this case the chain ends would experience a rapid, large excursion through the solvent, commonly referred to as whipping motion. Since this whipping motion would bring into play large viscous forces, suggestions have been put forward conjecturing various types of correlated motions such as the crankshaft of Schatzki,[2] the gauche migration of Helfand,[3] the three-bond motion,[4,5] and others which would serve to limit chain-end excursions.

A closely related question is the effect of correlated motions upon the activation energy for thermally activated conformational transitions. If rotations about bonds occur in an uncorrelated manner so that only one rotational energy barrier is crossed at a given time, the theory of thermally activated processes indicates that the activation energy for the process should be E_b, the height of the

0024-9297/81/2214-0785$01.25/0

rotational energy barrier. If the motion is correlated so that two or more barriers are surmounted at the same time, it appears that the activation energy would be increased correspondingly. For example, if correlation occurs by the Schatzki crankshaft mechanism, two barriers are crossed simultaneously and it would appear that the activation energy should be $2E_b$.

The reasoning may be summarized therefore in the following syllogism: (1) Uncorrelated rotations imply large chain-end excursions and high viscous drag. (2) The need to limit viscous drag implies correlated rotations such as crankshaft motions. (3) Correlated rotations imply an activation energy substantially greater than E_b, e.g., $2E_b$ for the crankshaft mechanism.

Morawetz and co-workers[6-9] have recently conducted a series of elegant experiments which clearly demonstrate that the conclusion of this reasoning is wrong. By use of fluorescence spectroscopy[6-9] and by the comparison of the quantum yields of photoisomerization in chain molecules and their analogues[7] they have measured the rates of barrier crossing in a long-chain molecule with many bonds and in an analogue molecule containing only a single rotational energy barrier of the same character as in the polymer. They found that the activation energies for the process in the polymer and in the analogue were identical within experimental error.

The experiments of Morawetz and co-workers raise the question as to which statement of the above syllogism is at fault and we wish to examine it here by the technique of computer simulation. This approach has been extensively used in recent years for the study of polymers in solution. The methods employed include Brownian dynamics,[10-18] molecular dynamics,[19-25] and Monte Carlo simulations.[26-30] In this paper we use the polymer model and calculation procedure developed by Pear and Weiner[17,18] (referred to hereafter as I and II) and attempt to parallel in the computer simulation the general approach taken by Morawetz and co-workers. That is, we compare simulated transition rates in a model of a long-chain molecule and in an analogue containing only a single rotational barrier.

The question of barrier crossing rates in polymers has been considered theoretically by Helfand[3] and, more recently, by Skolnick and Helfand[31] and by computer simulation by Helfand, Wasserman, and Weber.[13] Their work is based on flexible polymer models (bond lengths and bond angles are maintained nearly constant by stiff springs) whereas our work utilizes a polymer model of linked rigid bodies (fixed bond lengths and bond angles are imposed as geometric constraints). Some of our observations, nevertheless, particularly in regard to the localized nature of barrier crossing, are in agreement with their results. This study therefore serves, in part, to complement that of Helfand and co-workers by providing an indication of the role played by bond stretching and bending in the process.

A key aspect of the dynamics of long-chain molecules in solution is that the directions of motion in configuration space which minimize viscous drag do not, in general, coincide with those tangent to the paths of steepest descent along the potential energy surface. The viscous drag aspects have been emphasized in the recent work of Pear, Northrup, and McCammon.[32] In this work we study the interplay between viscous drag and energetic forces by means of a simple two-dimensional model.

The plan of the paper is as follows: A general description of the polymer model together with an outline of the numerical procedure used is given in section 1 and computer simulation results are presented in section 2. The simple two-dimensional model which permits controlled variation of the degree of correlation is described in section 3 together with computer simulation studies of its behavior. Conclusions are presented in section 4.

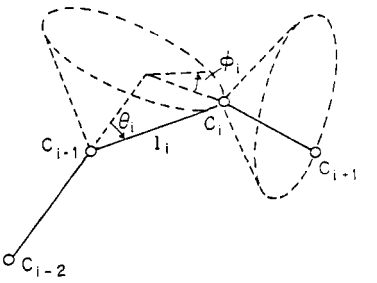

Figure 1. A section of backbone chain that depicts the notation used. Backbone atoms are represented by C_{i-2}, C_{i-1}, C_i, and C_{i+1}. A chain of N bonds has $N + 1$ atoms C_i, $N - 1$ valence angles θ_i, and $N - 2$ dihedral angles ϕ_i.

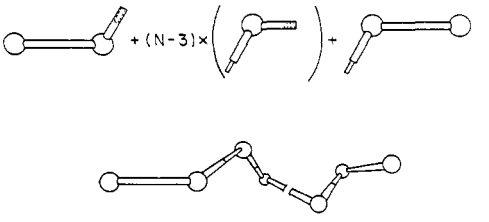

Figure 2. The mechanical system that corresponds to a rigid backbone chain. It maintains fixed bond lengths and valence angles. A pin on each body fits into a socket (dotted outline) of the previous body. This allows variations in the dihedral angles of the resulting chain.

1. Model Description

A complete description of this model is presented in I and only a general picture is given here. In order to introduce notation, consider the diagram of a backbone chain of atoms shown in Figure 1. The atom positions are given by C_{i-2}, C_{i-1}, C_i, and C_{i+1}. The bonds are described by a vector $\mathbf{l}_i$ running from C_{i-1} to C_i, the angle formed between $\mathbf{l}_i$ and $\mathbf{l}_{i-1}$ denotes the valence angle θ_i, and the rotation of $\mathbf{l}_i$ about an axis along $\mathbf{l}_{i-1}$ is measured by the dihedral angle ϕ_i. To form a rigid backbone chain with N bonds, the valence angles θ_i and bond lengths $|\mathbf{l}_i|$ are constrained to the constants θ and l. The $N - 2$ internal dihedral angles ϕ_i ($i = 3, ..., N$) are permitted to vary.

An equivalent mechanical system can be constructed as depicted schematically in Figure 2. Each link of the chain is composed of a single backbone atom to which are attached two massless connecting rods of length $l/2$ at an angle θ to each other. Joining these forms a chain of bond length l and valence angle θ. The ends of the chain are treated by considering each of the two end atoms and its nearest neighbor as one rigid body. Since the connecting hinges permit rotation only about an axis between two adjacent backbone atoms, the linked rigid body model eliminates variation in bond lengths and valence angles. However, it still allows conformation changes to take place by means of dihedral angle rotations.

This system has six degrees of freedom in addition to the internal degrees of freedom ϕ_i ($i = 3, ..., N$). These are the three degrees of freedom for the translational motion of the center of mass of the entire chain and the three angular coordinates that orient the first body of the chain with respect to some reference frame. In the numerical method presented in I, the translational coordinates produce separate equations of motion and are eliminated from

consideration. The angular coordinates are described by three Bryant angles ϕ_0, ϕ_1, ϕ_2 (similar to Euler angles) which depict the orientation as a rotation of ϕ_0 about the x axis of the reference frame followed by subsequent rotations of ϕ_1 and ϕ_2 about the new y and z axes, respectively. The chain is then described by the $N + 1$ dihedral angles $\phi_0, ..., \phi_N$. In the present paper, we will be concerned with the internal state of the chain and thus focus attention on the $N - 2$ dihedral angles $\phi_3, ..., \phi_N$.

In I, Pear and Weiner examined the differences between rigid and flexible models of 3-bond polymer chains that were freely rotating (i.e., with no hindering of the internal dihedral angle rotation). They found that the distribution of the single-variable dihedral angle ϕ was uniform for the flexible model and nonuniform for the rigid model. This was due to the metric determinant $g(\phi)$ introduced by bond length and valence angle constraints. Following a suggestion put forth by Fixman,[10] they demonstrated that the uniform distribution of the flexible model could be reproduced in the rigid model by the inclusion of a compensating potential $U(\phi_3) = k_B T \ln \{[g(\phi)]^{1/2}\}$. In II, Pear and Weiner conjectured a generalization of the Fixman potential for an N-bond chain in the form

$$U(\phi_3,...,\phi_N) = k_B T \sum_{i=3}^{N} \ln \{[g(\phi_i)]^{1/2}\} \qquad (1.1)$$

where g is the metric determinant of a 3-bond chain with the same valence angle and atomic masses as the long chain. It was found computationally that this potential produced the desired uniform distribution of dihedral angles $\phi_3, ..., \phi_N$ in the absence of other imposed rotational energy barriers and this generalized Fixman potential is incorporated as a torsional potential in the linked rigid body model.

To introduce the hindered rotation of dihedral angles caused by side-group interaction, we consider a piecewise quadratic potential with one barrier on the interval $[-\pi,\pi]$

$$V(\phi_i) = (2E_b/\pi^2)[(\phi_i - \phi_b) + \pi]^2 \qquad \phi_i - \phi_b < -\pi/2$$

$$V(\phi_i) = E_b - (2E_b/\pi^2)(\phi_i - \phi_b)^2 \qquad -\pi/2 \le \phi_i - \phi_b \le \pi/2$$

$$V(\phi_i) = (2E_b/\pi^2)[(\phi_i - \phi_b) - \pi]^2 \qquad \pi/2 < \phi_i - \phi_b \qquad (1.2)$$

E_b is the barrier height and ϕ_b determines the position of the barrier peak.

The behavior of this model, regarded as in thermal motion in dilute solution, was simulated by the technique of Brownian dynamics as detailed in I. As noted there, the equations of motion were developed on the basis of the formalism outlined by Wittenburg[33] for treating the dynamics of systems of linked rigid bodies. Our interest in the present work is not the direct quantitative comparison with experiment but rather in the general nature of the dynamics of this type of system. For this reason, we work with valence angles of 90° and the single-barrier rotational potential.

2. Simulation Results

In Figures 3 and 4, we present Arrhenius plots for chains of $N = 3$, 7, and 15 bonds with $\eta = 2.0$ and for $N = 3$ and 15 bonds with $\eta = 4.0$.[34] Rates for each dihedral angle were measured by counting only those transitions that crossed the entire barrier region, i.e., those that traversed the region $\phi_b - \pi/2$ to $\phi_b + \pi/2$. After the number of jumps for each angle were divided by the total time, the resulting individual rates were averaged to produce an overall rate. A least-squares fit was used to determine the activation

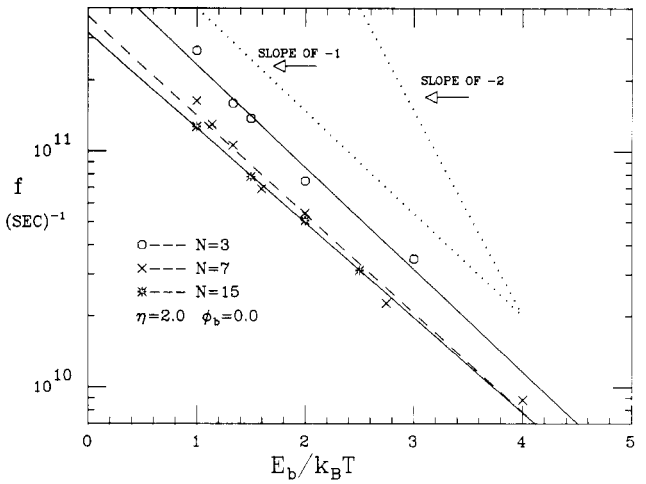

Figure 3. Arrhenius plot for chains of varying length. The frequency f represents the number of complete transitions per second. The barrier height $E_b = 0.5$, the viscosity $\eta = 2$, and the time step for the simulation $\delta t = 0.05$ are all in dimensionless units.[34] A slope of −1 corresponds to an activation energy of $1E_b$.

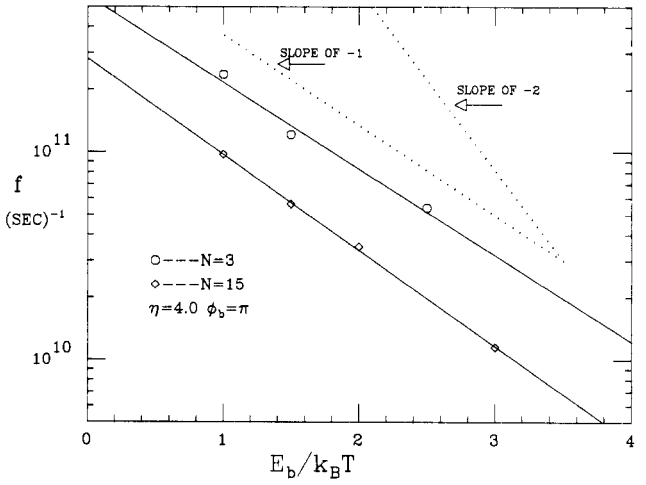

Figure 4. Arrhenius plot for chains of 3 and 15 bonds, respectively, and $\eta = 4$.

energies for each chain. As clearly seen from the comparison slopes, the activation energies for each chain show an activation energy of $1E_b$ (within 10%). There is also a decrease in the frequency factors with increasing chain length. The experimental work of Morawetz and coworkers[6-9] demonstrates similar behavior; a chain with many dihedral angles has the same activation energy as that for an analogue molecule with only one dihedral angle. Experiment also shows the lowered frequency factor for the long chain although the frequency factor reduction observed experimentally is only about 30% of that observed in the computer simulation. An additional feature to note is that there is a rapid approach to the behavior of the infinite chain. In the recent work of Skolnick and Helfand,[31] the transition rates of a central bond for chains of various conformations are examined. They find that the motion over a rotational barrier of a central bond is highly localized. That is, the accompanying motion of adjacent bonds decays rapidly in amplitude with distance from the central bond. Therefore there is a rapid approach to the behavior of the infinite chain for the transition rates of central bonds. This aspect of the process is confirmed by the present computer simulation.

A histogram of transition rates as a function of individual angles for a 15-bond chain is presented in Figure 5. This picture shows an increase in rates as one proceeds

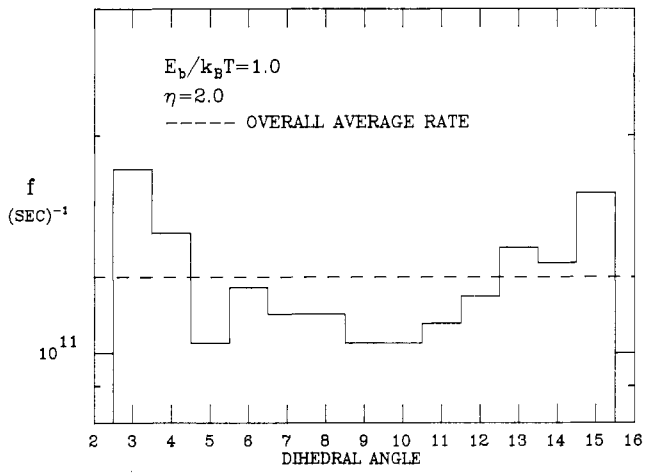

Figure 5. Histogram of transition rates as a function of individual angles along chain for a 15-bond chain.

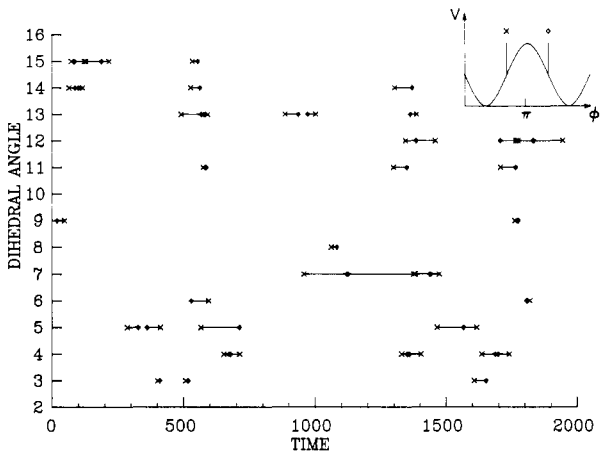

Figure 6. Times at which individual angles begin and end transitions across barrier for a 15-bond chain. $E_b/k_BT = 3$, $\eta = 4$, and $\delta t = 0.05$ (dimensionless units). The rotational energy barrier was at $\phi_b = \pi$. The insert in the upper right-hand corner relates the symbols × and ◊ to the points crossed on the potential barrier.

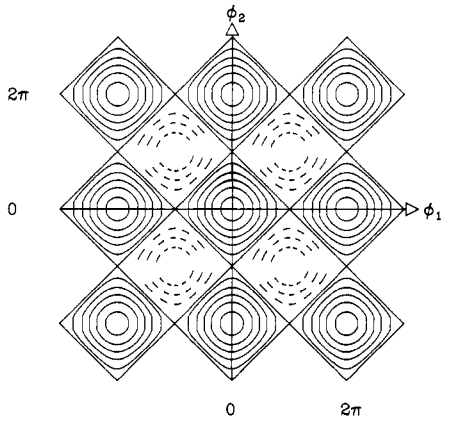

Figure 7. Contour plot of the potential of eq 3.2. Dashed lines are neighborhoods of maxima and solid lines those of minima. $V = 0$ for minima, $V = 2E_b$ for maxima, and $V = E_b$ for saddle points.

from the interior of the chain toward the ends. This result also appears to be in accord with the localized nature of barrier crossing noted in the theory of Skolnick and Helfand;[31] rates for bonds near the center are lower than those near the ends since the barrier crossing must be accompanied by the small-amplitude motion of bonds to either side.

The qualitative agreement of the simulation with both experiment and theory suggests that the model contains the essential features of the process. It is important to note that since the simulation utilizes a rigid model, accommodation of the chain by bond stretching and bending is not an essential aspect of the process. We can now examine the implications posited in the introduction.

(1) In II, Pear and Weiner examined the effect of viscosity on a chain that had one of the end bodies fixed in order to eliminate the effect of the rigid body rotation of the chain as a whole. This enabled them to concentrate on the motion of the chain end due to internal motions. The motion of the free end relative to the fixed end was found to decrease with increases in viscosity. In a model chain for which the variations of dihedral angles were uncorrelated, changes in viscosity were found to produce little effect and large chain end excursions were noted.

(2) To see that some form of coordinated motion takes place in the free chain, records were kept in the present computations of the times at which individual dihedral angles crossed their rotational barriers. Typical results are shown in Figure 6. There we plot a sequence of transitions vs. time for a 15-bond chain with $\eta = 4$ and $E_b/k_BT = 3$. This value of E_b/kT was chosen in order to obtain a suitable sampling of barrier crossings in a reasonable length of computer run, although a somewhat larger value, $E_b/kT \sim 5$, is more realistic for paraffin chains. Each jump (which, as described for the rate plots, must clear the entire barrier region to be counted) is represented by a line connecting the times when it enters and leaves the barrier region. Different symbols are used at each end of the barrier so that the direction in which the barrier was crossed may be noted. One purpose in obtaining records of this type was to determine whether hindered rotations propagated along the chain in a regular sequence, somewhat in analogy to the manner in which a dislocation propagates in a crystal. This was not observed in these simulations. However, the results do show a high degree of simultaneity and cooperativity in the motion of the dihedral angles. Yet, at the same time, Figures 3 and 4 demonstrate an activation energy of only $1E_b$. To return to the syllogism of the Introduction, it would seem that implication 3, which states that coordinated motion implies an activation energy of a multiple of E_b, is at fault.

In order to gain further insight into the role of viscosity in producing correlated barrier crossings and the subsequent effect upon the activation energy of the process, we turn in the next section to a simple model system.

3. Two-Dimensional Model

We next consider as a simplified model a particle with two degrees of freedom, where each degree of freedom represents an internal dihedral angle of a polymer. It obeys a Langevin equation of the form

$$\ddot{\phi}_i = -\partial V/\partial \phi_i - \eta_{ij}\dot{\phi}_j + R_i(t) \quad (i, j = 1, 2; \text{ sum over } j) \tag{3.1}$$

where

$$V(\phi_1,\phi_2) = (E_b/2)(2 - \cos \phi_1 - \cos \phi_2) \tag{3.2}$$

η_{ij} is a viscosity tensor and $R_i(t)$ is the random Langevin force term. The superposed dot denotes differentiation with respect to time. A contour plot of the potential is shown in Figure 7, where dashed lines represent the neighborhood of a maximum and solid lines that for a minimum. The maxima have $V = 2E_b$, the minima have $V = 0$, and there are saddle points located at the intersection of the equipotential lines $\phi_2 = (2n + 1)\pi - \phi_1$, ϕ_2

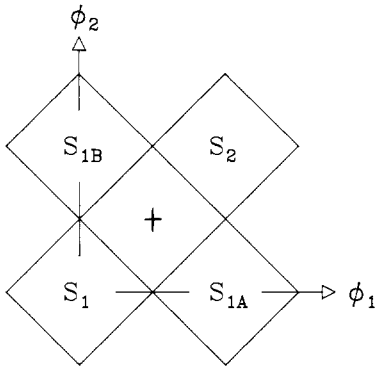

Figure 8. Schematic depiction of the types of transitions that can occur for the potential of eq 3.2. Transitions S_1–S_{1A} or S_1–S_{1B} are uncorrelated jumps; transitions S_1–S_2 are correlated.

$= (2n + 1)\pi + \phi_1$ ($n = 0, \pm1, \pm2, ...$) with $V = E_b$.

To motivate the use of this model, consider the diagram of Figure 8. This is a schematic depiction of the possible transitions from one minimum to another that can occur for the potential of eq 3.2. These transitions can be classified into two groups: (1) the equivalent passages S_1 to S_{1A} or S_1 to S_{1B}, which are uncorrelated jumps, or (2) passages from S_1 to S_2, which are correlated jumps with ϕ_1 and ϕ_2 simultaneously moving from one energy minimum to another.

From the energetic viewpoint, uncorrelated jumps over the saddle points with $V = E_b$ are favored as opposed to correlated jumps over barrier peaks with $V = 2E_b$. We wish to consider variations in the viscosity tensor η_{ij} so that viscous drag is minimized for correlated jumps when it is suitably defined. For this purpose it is convenient to postulate that η_{ij} is diagonal in the orthogonal coordinate system

$$y_1 = (1/\sqrt{2})(\phi_1 + \phi_2) \tag{3.3a}$$

$$y_2 = (1/\sqrt{2})(\phi_1 - \phi_2) \tag{3.3b}$$

In this reference frame, the Langevin equations take the form

$$\ddot{y}_1 = -\eta_1\dot{y}_1 - \sqrt{2}E_b \sin(y_1/\sqrt{2}) \cos(y_2/\sqrt{2}) + A_1(t) \tag{3.4a}$$

$$\ddot{y}_2 = -\eta_2\dot{y}_2 - \sqrt{2}E_b \cos(y_1/\sqrt{2}) \sin(y_2/\sqrt{2}) + A_2(t) \tag{3.4b}$$

where η_1 and η_2 are coefficients of viscosity in the y_1 and y_2 directions, respectively. $A_1(t)$ and $A_2(t)$ are normally distributed random forces with the statistical properties

$$\langle A_i(t)\rangle = 0 \tag{3.5a}$$

$$\langle A_1(t)A_1(t')\rangle = 2\eta_1 T\delta(t - t')$$
$$\langle A_2(t)A_2(t')\rangle = 2\eta_2 T\delta(t - t') \tag{3.5b}$$

with T being a dimensionless temperature.

In the y_1, y_2 frame it is easy to see that by varying η_1 and η_2, we can control the nature of viscous drag on the system. Depending on their values, there will be a maximum drag along one of the axes and a minimum drag along the other, with gradations in the strength of the viscosity between the two. For example, $\eta_1 = \eta_2$ yields an isotropic medium with constant drag in all directions, whereas for $\eta_1 \neq \eta_2$ ($\eta_2 > \eta_1$), the medium is anisotropic and has an axis of easy motion along y_1. There is no preferred direction of motion for the isotropic situation; hence the topology of the potential energy function should be the dominant factor in determining the types of transitions that occur. For the anisotropic case, there is a direction of easy motion (in terms of viscous forces) that is not aligned with a direct path between adjacent minima but rather is at an angle of 45° to it. Since a transition from S_1 to S_2 (Figure 8) must take place in some way parallel to the y_1 axis, one expects that a medium with y_1 as the axis of least drag has the greatest likelihood of producing correlated jumps.

To display the form of the viscosity tensor of eq 3.1, we transform back to the ϕ_1, ϕ_2 frame. This yields

$$\eta_{ij} = \tfrac{1}{2}(\eta_1 + \eta_2) \qquad i = j$$
$$= \tfrac{1}{2}(\eta_1 - \eta_2) \qquad i \neq j \tag{3.6}$$

The random force terms, $R_i t$, are composite random variables comprised of orthogonal combinations of the $A_i(t)$. These have the statistical properties

$$\langle R_i(t)\rangle = 0 \qquad \langle R_i(t')R_i(t)\rangle = (\eta_1 + \eta_2)T\delta(t - t') \tag{3.7a}$$

$$\langle R_1(t)R_2(t')\rangle = (\eta_1 - \eta_2)T\delta(t - t') \tag{3.7b}$$

Note that the $R_i(t)$ are correlated. This is a consequence of the viscous coupling. As a check, for an isotropic medium, the equations should revert to that for simple Brownian motion, and indeed, for $\eta_1 = \eta_2 = \eta$, the viscosity tensor is diagonal, the correlation of the force terms is zero, and the autocorrelation becomes $2\eta T$. Thus, the ϕ_1, ϕ_2 frame is seen to be most useful for considering the potential energy surface, trajectories, and transitions, while the y_1, y_2 frame enables us to better visualize the effects of viscous forces.

It is not our intention with this model to represent a molecule moving in a solvent whose viscosity is anisotropic. Rather, the model is intended to represent, in a highly idealized way, the motion of a long-chain molecule in a solvent with the usual isotropic viscosity. In this latter case, uncorrelated motion results in tail whipping and high viscous drag, while highly correlated motion which suppresses tail whipping results in low viscous drag. Uncorrelated motion and correlated motion represent two distinct types of paths in the multidimensional configuration space of the long-chain molecule. Our model focuses on these two paths and the anisotropic viscosity tensor mimics the difference in drag between the two.

The numerical procedure employed to produce a representative trajectory of the system was a stochastic extension of the Runge–Kutta method developed by Helfand[35] and used to second order. The form of the y_1, y_2 Langevin equations (eq 3.4a and 3.4b) lend themselves most readily to this procedure. To ensure the efficacy of the simulation, a time average was made of the kinetic energy of the system and compared to the equipartition value of $2(T/2)$. For suitable choices of the time step δt, trajectories could be generated such that the kinetic energy behaved properly and for most calculations $\delta t = 0.05$ was employed. The procedure was as follows for each trajectory. A random initial position was chosen subject to the condition that it was in the well at the origin (i.e., $|\phi_1| < \pi$, $|\phi_2| < \pi$); initial velocities were taken to be zero. These values were converted to the y_1, y_2 system and by means of the stochastic Runge–Kutta method, new values incremented in time by δt were obtained. For the purpose of calculating rates, the y_1, y_2 values were expressed as ϕ_1, ϕ_2 values at each time step and transitions were counted by the method used for the chain simulation.

Figure 9 shows Arrhenius plots for an isotropic medium ($\eta_1 = \eta_2 = 4$) and one that is anisotropic ($\eta_1 = 0$, $\eta_2 = 8$). In both cases the activation energy is E_b within ±10%, where, as previously noted, E_b corresponds to the saddle point energy.

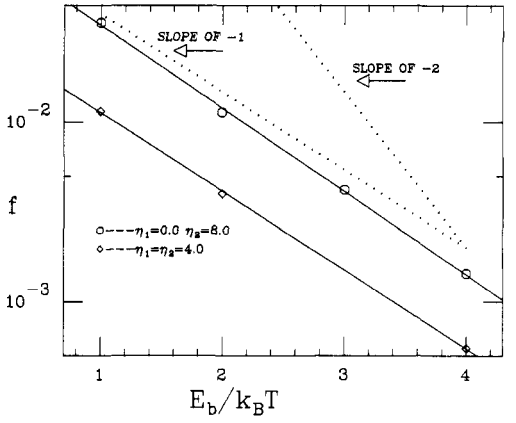

Figure 9. Arrhenius plot for the two-dimensional model system. All quantities are dimensionless. $E_b = 2$ and $\delta t = 0.05$. A slope of −1 corresponds to an activation energy of $1E_b$.

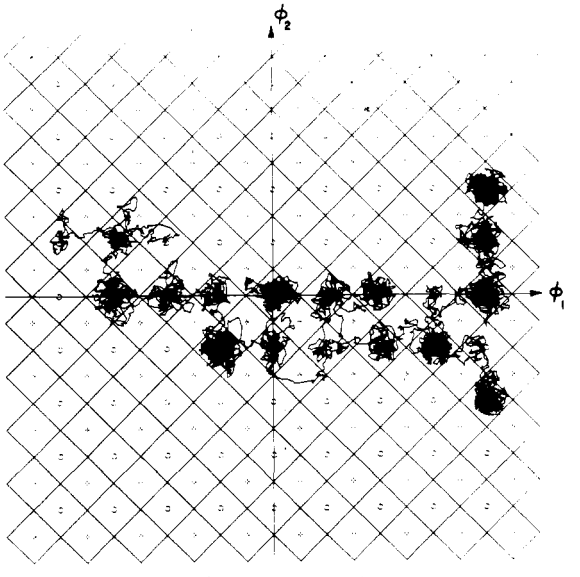

Figure 10. Trajectory plot for the two-dimensional system with isotropic viscosity ($\eta_1 = 4$, $\eta_2 = 4$). $E_b/k_BT = 3$ and $\delta t = 0.05$. The trajectories are from a portion of a representative simulation. Maxima are marked by crosses and minima by circles. Note that the trajectory shows no preferred direction of motion and that the transitions are uncorrelated in nature (i.e., of the S_1–S_{1A} or S_1–S_{1B} type).

Clearly, the two systems are not differentiated by their respective activation energies. What must now be considered is whether or not they differ in the types of transitions being undergone. To answer this question, we present a trajectory plot for each case in order to demonstrate how passages between minima are negotiated. In Figures 10 and 11, we show trajectory plots for the isotropic and anisotropic systems, respectively. $E_b/k_BT = 3$ for both systems, with the only difference between the two simulations being the viscosity tensor. The difference in character between the two plots is apparent. In Figure 10, the isotropic case, there appears to be no preferred direction in the overall motion. In transitions between adjacent minima the passage generally takes place through the saddle point along the path of steepest descent on the energy surface. Transitions between minima of the S_1 to S_2 type (Figure 8) do not seem to take place. Thus, the isotropic system demonstrates uncorrelated behavior. However, for the anisotropic case, as seen in Figure 11, the motion takes place parallel to the y_1 direction and many coordinated jumps are in evidence. Here, too, the transitions take place through the saddle point but the crossing

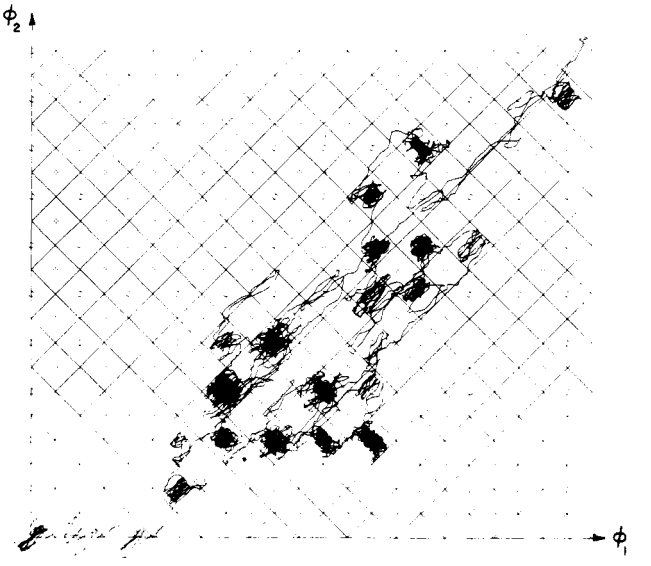

Figure 11. Trajectory plot for the two-dimensional system with anisotropic viscosity ($\eta_1 = 0$, $\eta_2 = 8$). All parameters are the same as those for the isotropic system of Figure 10 except for the viscosity. This system has an axis of zero drag along the y_1 axis (which is rotated 45° counterclockwise from the positive ϕ_1 axis). Note that motion is aligned along the y_1 axis and that there is a mixture of correlated (S_1–S_2) and uncorrelated (S_1–S_{1A}, S_1–S_{1B}) transitions.

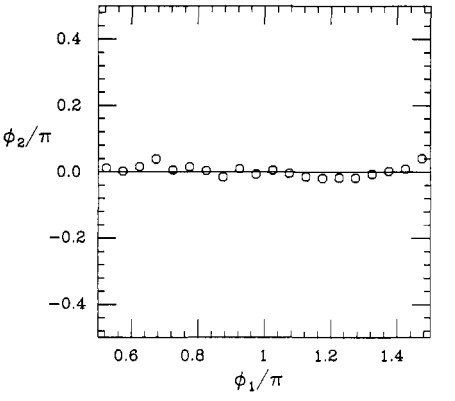

Figure 12. Plot depicting the average of many passages through the saddle point for the isotropic medium. $E_b/k_BT = 3$, $\eta_1 = \eta_2 = 4$, and $\delta t = 0.05$. The horizontal line $\phi_2 = 0$ is the path of steepest descent through the saddle point (located at $\phi_1 = \pi$, $\phi_2 = 0$).

takes place generally along the equipotential lines $\phi_2 = (2n + 1)\pi + \phi_1$ ($n = 0, \pm1, \pm2, \ldots$). Hence, the anisotropic system demonstrates correlated behavior.

In Figure 12, we show a plot depicting the average of many passages through the saddle point for the isotropic case. This plot was produced in the following manner. As ϕ_1 underwent a jump, the values of ϕ_1 and ϕ_2 were stored. When the jump was completed, the values of ϕ_2 (after reduction to the interval $-\pi < \phi_2 < \pi$) were put into bins corresponding to their respective ϕ_1 positions. These values were averaged with those for subsequent jumps to yield Figure 12. Clearly, this figure shows that the passage through the saddle point occurred, on the average, in the direction describing the path of steepest descent through the saddle point. Similar results were found for transitions in the ϕ_2 direction.

The more interesting case is the resultant motion for the anisotropic system. By making y_1 the direction of least drag (specifically zero drag), the overall motion of the system becomes aligned with the y_1 axis. Again, motion

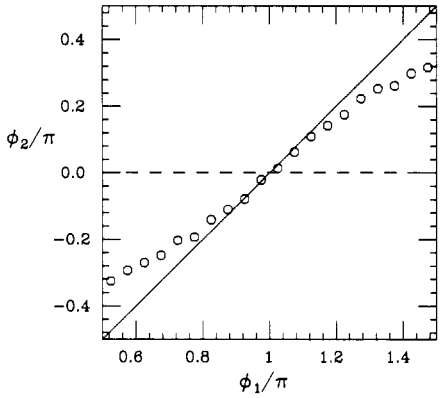

Figure 13. Plot depicting the average of many passages through the saddle point for the anisotropic medium. $E_b/k_BT = 3.0$, $\eta_1 = 0$, $\eta_2 = 8$, and $\delta t = 0.05$. The diagonal line is the equipotential line $V = E_b$ and the saddle point is at $\phi_1 = \pi$, $\phi_2 = 0$. Note that passages are through the saddle point but aligned along the line $V = E_b$. The falloff from this line at the ends is representative of the fact that not all transitions are correlated ones.

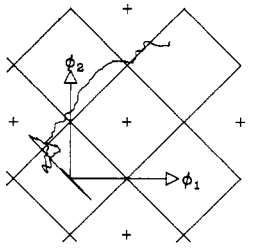

Figure 14. Trajectory plot showing the early evolution of the system for the anisotropic case ($\eta_1 = 0$, $\eta_2 = 8$). This shows how the direction of motion is transferred from the y_2 axis to the y_1 axis. $E_b/k_BT = 3$ and $\delta t = 0.05$. The initial positions were $\phi_1 = 0.02$, $\phi_2 = 0.03$ with initial velocities set equal to zero.

appears to be distributed about a path that passes through the saddle point but not along the path of steepest descent of the potential surface. Rather, the energetics of the potential seem to combine with the anisotropic viscosity to produce a reaction coordinate that lies along the equipotential line $V = E_b$ (in the direction of y_1) that leads from one minimum to another, nonadjacent, one. This is demonstrated in the plot of Figure 13 (produced in the same manner as Figure 12). The straight line in this figure represents the line $V = E_b$.

The Brownian dynamics of this model has an interesting, counterintuitive aspect. Consider the case with $\eta_1 = 0$ and $\eta_2 > 0$ for example. The random force, which provides the impulse for the particle's motion, then has zero component in the y_1 direction; yet the predominant direction of motion in this case is in that direction, as may be seen from Figure 13. The resolution of this paradoxical behavior is the coupling provided by the potential V. This coupling turns the particle from the y_2 direction, in which the random force acts but in which the drag is high, into the y_1 direction, in which the drag vanishes. The gradient of the potential V in the y_1 direction vanishes on trajectories $y_1 = 2^{1/2}n\pi$, $n = 0, \pm1, \ldots$, as seen from eq 3.4a and motion along these particular trajectories would not be turned into the y_1 direction. For example, a simulation initiated at the origin with zero initial velocities will execute Brownian motion along y_2 with no y_1 component of motion. The turning effect can be observed by initiating the simulation near, but not at, the origin and observing the subsequent trajectory. This is shown in Figures 14 and 15. In Figure 14, the initial state is at $\phi_1 = 0.02$, $\phi_2 = 0.03$ and in Figure 15, it is at $\phi_1 = 0.2$, $\phi_2 = 0.3$. The turning effect operates

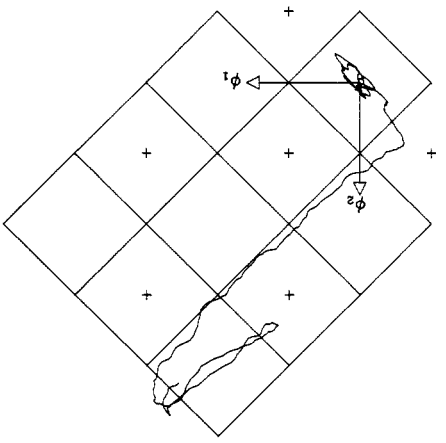

Figure 15. Trajectory plot for the same situation as described for Figure 14 but with initial positions $\phi_1 = 0.2$, $\phi_2 = 0.3$. Note that the motion is not as strongly aligned along the y_2 axis in the initial stages as is the case for Figure 14. This is due to the stronger initial turning effect due to starting higher on the potential surface.

in both cases but begins more rapidly in the second case.

4. Conclusions

The Brownian dynamics simulation of a linked rigid body model of a linear polymer in solution shows good agreement with the recent experimental results of Liao and Morawetz[9] in two important respects: (1) the activation energy for rotational barrier crossing is the same for a long-chain molecule and for an analogue with only one rotational barrier and (2) the frequency factor shows a slight decrease with increasing chain length.

The fact that these simulations were carried out on the basis of a rigid polymer model (bond length and valence angle fixed) demonstrates that it is not essential to include bond stretching and bond bending in order to explain the experimental results. In this sense the present results are complementary to those of Skolnick and Helfand[31] and of Helfand, Wasserman, and Weber,[13] which are based on flexible models. It should be emphasized that although our results show that a rigid model exhibits behavior consistent with the experimental results, they do not serve to measure the importance or the role of molecular flexibility in the dynamics of real molecules.

An examination of the details of these computer simulation results shows the presence of many barrier crossings which occur with near simultaneity. It appears, therefore, that the intuitive expectation that correlated barrier crossing should lead to an activation energy which is a multiple of a single barrier height is not correct.

In order to gain further insight into the interplay between viscous drag and energetic forces in this process, we have constructed a simple model consisting of a particle with two degrees of freedom subject to energetic forces derived from a potential and to drag forces due to a tensor viscosity. Each degree of freedom of the particle is regarded as representing the motion of a dihedral angle over an energy barrier[36] and, by the variation of the definition of the viscosity tensor, it is possible to have the effect of viscous drag favor either uncorrelated or correlated passage over energy barriers. The model was studied by Brownian dynamics and the activation energy for barrier crossing in this model was found to be the same for an isotropic viscosity tensor which favors uncorrelated barrier crossings and for a highly anisotropic viscosity tensor which favors correlated barrier crossings. The two-dimensional model exhibits, therefore, the same insensitivity of the activation energy to barrier-crossing correlation which is observed in the polymer model. For the two-dimensional model,

however, it was possible to make a more detailed study of the particle trajectories during barrier crossings. It was found that for both cases (isotropic and highly anisotropic viscosity tensor) barrier crossings occurred over a saddle point with energy equal to one barrier height. In the isotropic case the average path followed was one of steepest descent on the energy surface and corresponded to uncorrelated barrier crossing. In the anisotropic case, however, the average path followed through the saddle point was a constant-energy path and corresponded to correlated motion of the two "dihedral angles" but with a phase lag between them. These average paths help make understandable the insensitivity of the activation energy for the two-dimensional model. It remains for future work to determine the extent to which these ideas are applicable to long-chain molecules.

Acknowledgment. The computations were carried out on the Brown University Division of Engineering VAX-11/780 computer. The acquisition of this computer was made possible by grants from the NSF (Grant No. ENG78-19378), the General Electric Foundation, and the Digital Equipment Corp. We thank Dr. H. Morawetz and Bao Nguyen for rewarding discussions.

References and Notes

(1) This paper is based on the research of D. Perchak performed in partial fulfillment of the requirements for the Ph.D. in Physics at Brown University. This work has been supported by the Gas Research Institute (Grant No. 5080-363-0309) and by the National Science Foundation through the Materials Research Laboratory, Brown University.
(2) Schatzki, T. F. *J. Polym. Sci.* **1962**, *57*, 496. *J. Polym. Sci., Part C* **1966**, *14*, 139.
(3) Helfand, E. *J. Chem. Phys.* **1971**, *54*, 4651.
(4) Valeur, B.; Jarry, J.-P.; Geny, F.; Monnerie, L. *J. Polym. Sci., Polym. Phys. Ed.* **1975**, *13*, 667. Valeur, B.; Monnerie, L.; Jarry, J.-P. *Ibid.* **1975**, *13*, 675.
(5) Jones, A. A.; Stockmayer, W. H. *J. Polym. Sci., Polym. Phys. Ed.* **1977**, *15*, 847.
(6) Morawetz, H. *Science* **1979**, *203*, 405. *Pure Appl. Chem.* **1980**, *52*, 277.
(7) Chen, D. T.-L.; Morawetz, H. *Macromolecules* **1976**, *9*, 463.
(8) Liao, T.-P.; Okamoto, Y.; Morawetz, H. *Macromolecules* **1979**, *12*, 535.
(9) Liao, T.-P.; Morawetz, H. *Macromolecules* **1980**, *13*, 1228.
(10) Fixman, M. *J. Chem. Phys.* **1978**, *69*, 1527. *Ibid.* **1978**, *69*, 1538.
(11) Weber, T. A. *J. Chem. Phys.* **1978**, *69*, 2347. *Ibid.* **1979**, *70*, 4277.
(12) Helfand, E. *J. Chem. Phys.* **1978**, *69*, 1010.
(13) Helfand, E.; Wasserman, Z. R.; Weber, T. A. *J. Chem. Phys.* **1979**, *70*, 2016. *Macromolecules* **1980**, *13*, 526.
(14) McCammon, J. A.; Northrup, S. H.; Karplus, M.; Levy, R. M. *Biopolymers* **1980**, *19*, 2033.
(15) Evans, G. T.; Knauss, D. C. *J. Chem. Phys.* **1980**, *72*, 1504.
(16) Weiner, J. H.; Pear, M. R. *Macromolecules* **1977**, *10*, 317.
(17) Pear, M. R.; Weiner, J. H. *J. Chem. Phys.* **1979**, *71*, 212, hereafter referred to as I.
(18) Pear, M. R.; Weiner, J. H. *J. Chem. Phys.* **1980**, *72*, 3939, hereafter referred to as II.
(19) Rebertus, D. W.; Berne, B. J.; Chandler, D. *J. Chem. Phys.* **1979**, *70*, 3395.
(20) Ryckaert, J.-P.; Bellemans, A. *Chem. Phys. Lett.* **1975**, *30*, 123.
(21) Weber, T. A.; Helfand, E. *J. Chem. Phys.* **1979**, *71*, 4760.
(22) Montgomery, J. A., Jr.; Holmgren, S. L.; Chandler, D. *J. Chem. Phys.* **1980**, *73*, 3688.
(23) Bishop, M.; Kalos, M. H.; Frisch, H. L. *J. Chem. Phys.* **1979**, *70*, 1299.
(24) Rapaport, D. C. *J. Chem. Phys.* **1979**, *71*, 3299.
(25) Gotlib, Yu. Ya.; Balabaev, N. K.; Darinskii, A. A.; Neelov, I. M. *Macromolecules* **1980**, *13*, 602.
(26) Gō, N.; Scheraga, H. A. *Macromolecules* **1978**, *11*, 552.
(27) Verdier, P. H.; Stockmayer, W. H. *J. Chem. Phys.* **1962**, *36*, 227.
(28) Verdier, P. H. *J. Chem. Phys.* **1979**, *70*, 5708.
(29) Okamoto, H. *J. Chem. Phys.* **1979**, *70*, 1690.
(30) Baumgartner, A.; Binder, K. *J. Chem. Phys.* **1979**, *71*, 2541.
(31) Skolnick, J.; Helfand, E. *J. Chem. Phys.* **1980**, *72*, 5489.
(32) Pear, M. R.; Northrup, S. H.; McCammon, J. A. *J. Chem. Phys.* **1980**, *73*, 4703.
(33) Wittenburg, J. "Dynamics of Systems of Rigid Bodies"; Teubner: Stuttgart, 1977.
(34) Units used are dimensionless. They correspond to a system where the mass of a carbon atom, the length l of a C–C bond, and $k_B T_{ref}$, where T_{ref} = 600 K, are all unity. A δt of 1 corresponds to 7.51×10^{-14} s and a value of the coefficient η of 1 corresponds to 2.67×10^{-10} dyn/(cm s^{-1}) in cgs units. Note that this coefficient η, which multiplies atom velocity in the Langevin equation to yield the frictional force acting upon it, is not the solvent viscosity μ; it is obtained from the latter by a relation such as Stokes' law, $\eta = 6\pi a\mu$, where a is an effective atomic radius.
(35) Helfand, E. *Bell Syst. Tech. J.* **1979**, *58*, 2289.
(36) In this connection, see Blomberg (Blomberg, C. *Chem. Phys.* **1979**, *37*, 219), who focuses on two dihedral angles in his rate theory discussion. In particular, compare his Figure 4 and our Figure 7.

Influence of Counterion Exchange on the Induced Dipole Moment and Its Relaxation for a Rodlike Polyion

W. van Dijk, F. van der Touw, and M. Mandel*

Department of Physical Chemistry, Gorlaeus Laboratories, University of Leiden, 2300 RA Leiden, The Netherlands. *Received September 29, 1980*

ABSTRACT: The influence of the exchange between associated and free counterions on the distribution of the former along a uniformly charged, one-dimensional rod in the presence of a vanishingly small electric field has been investigated. The *two-phase model* has been used together with simplifying boundary conditions, and counterion–counterion as well as polyion–polyion interactions have been neglected. Expressions for the induced dipole moment in the associated phase and its relaxation time have been evaluated. Therein appears a characteristic length Z representing the ratio of the diffusion coefficient of the associated counterions in the axial direction along the rod to the rate of exchange. For a rod of length L these expressions reduce to those obtained from an analogous model in which exchange is neglected if $Z \gg L$. The induced dipole moment and its relaxation time are then proportional to L^3 and L^2, respectively. In the opposite case where $Z \ll L$ the value of the induced dipole moment is strongly reduced and proportional to L whereas the relaxation time is determined solely by the rate of exchange and is independent of L. It is thus demonstrated that such an exchange should have a considerable influence on the dielectric properties of polyelectrolyte solutions.

Introduction

Several theories have already been proposed to explain the contribution of linear polyelectrolytes in the ionized state to the electric polarization of their aqueous solutions. Many of them were based on a simplified model (the so-called two-phase model of Oosawa[1]) and the polarization

0024-9297/81/2214-0792$01.25/0